 https://doi.org/10.3311/PPme.21159

Periodica Polytechnica Mechanical Engineering, 67(1), pp. 70–80, 2023

Cause Analysis of Rail Corrugation Based on Stick-slip Characteristics

Zhiqiang Wang[1*], Zhenyu Lei[1]

[1] Institute of Rail Transit, Tongji University, No. 4800 Cao'an Road, 201804 Shanghai, China
[*] Corresponding author, e-mail: 1733359@tongji.edu.cn

Received: 11 September 2022, Accepted: 05 December 2022, Published online: 16 January 2023

Abstract

By analyzing the measured corrugation data, the cause of rail corrugation was discussed theoretically. Then, the vehicle-track coupling model was used to study the stick-slip characteristics of wheel-rail system. Finally, the cause of rail corrugation was explained by combining modal analysis and wheel-rail stick-slip relation. The transverse stick-slip curve on the inner rail-inner wheel of the leading wheelset presents a negative slope characteristic, which makes the inner wheel easy to slide on the inner rail surface and aggravates the wear of inner rail; there are also negative slope sections of the stick-slip curve on the outer rail-outer wheel of the trailing wheelset, but the adhesion coefficient is relatively large, indicating that the outer wheel will not slide obviously and the wear is relatively small. Meantime, with the increase of line curve radius, the negative slope phenomenon of stick-slip curves on the inner and outer rail sides shows a decreasing trend, which illustrates that the sliding wear of wheel is gradually reduced, and thus the occurrence probability of rail corrugation decreases. Combined with modal analysis, it can be seen that the coupling action of wheel discs bending vibration and inner rail bending-torsional vibration is the main cause of rail corrugation under the condition of wheel-rail system with stick-slip negative slope.

Keywords

corrugation, stick-slip characteristics, negative slope, modal analysis, coupling vibration

1 Introduction

Rail corrugation is a kind of longitudinal periodic damage on rail surface, which appears in railway systems all over the world. According to the wavelength-fixed mechanism and damage mechanism [1], rail corrugation can be divided into the following six types: roaring rails, rutting, other P2 resonance, heavy haul, light rail, and track form-specific. Since the discovery of rail corrugation, the related research has lasted for more than 100 years, but there is no effective method to prevent and control rail corrugation. Rail grinding is the most common treatment measure. However, while reducing the corrugation, it inevitably increases the maintenance cost and decreases the service life of the rail. Therefore, it is very meaningful to investigate the causes of rail corrugation and find out the effective measures to restrain this phenomenon.

Rail corrugation is particularly universal on small curve lines. When the vehicle runs through the corrugation section, it is easy to cause the abnormal vibration of vehicle and track components, reduce the stability of train operation and pose a hidden danger to the traffic safety. As for the causes of rail corrugation, scholars around the world have carried out a lot of research and put forward many theories, such as wear corrosion [2], uneven plastic deformation [3], wheel-rail resonance [4–9] and stick-slip vibration [10, 11], etc. However, the above theories can only explain some special cases of rail corrugation, and cannot explain the general phenomenon that most corrugations occur in the curve section. In addition, some scholars have also studied the generation and development characteristics of rail corrugation from the perspective of initial rail surface irregularities [12] and wheel-rail vertical resonance caused by rail surface irregularities [13]. Nevertheless, subsequent studies have shown that the initial irregularity is not a sufficient condition for the generation of rail corrugation. If the wheel-rail normal force is disturbed enough, the corrugation will still form [14].

For the control measures of rail corrugation, in addition to rail grinding, methods such as applying rail friction

Cite this article as: Wang, Z., Lei, Z. "Cause Analysis of Rail Corrugation Based on Stick-slip Characteristics", Periodica Polytechnica Mechanical Engineering, 67(1), pp. 70–80, 2023. https://doi.org/10.3311/PPme.21159

modifier [15], changing train operation speed distribution [16] and installing vibration-absorption structure [17] have also been widely used. However, the formation mechanism for rail corrugation is still unknown [18]. As mentioned above, scholars have proposed different theories for rail corrugation, but so far there is no general theoretical model to explain all the corrugation phenomena [19]. Why most of the corrugations occur in the curve section and most of them are distributed on the top surface of inner rail are still difficult problems for the railway industry.

Based on the above analysis, this paper focuses on the cause of rail corrugation. Firstly, the cause of rail corrugation is analyzed theoretically based on the measured data. Then, using the multi-body dynamics theory, the vehicle-track coupling model is constructed, and the stick-slip characteristics of wheel-rail system under different curvature radii are studied. Finally, by establishing three-dimensional solid finite element model of wheelset-track system and carrying out modal analysis, combined with the wheel-rail stick-slip relation, the formation reason of rail corrugation is explained.

2 Investigation on the cause of rail corrugation

2.1 Measured corrugation on the line

The measured section is located in a metro line in Tianjin, which was put into operation in April 2018, and the train adopts 6A marshalling. The ZX-2 type of track fastener is used in the measured section, whose vertical, transverse and longitudinal stiffnesses are 40 kN/mm, 9 kN/mm and 9 kN/mm, respectively, and the vertical, transverse and longitudinal dampings are 6400 Ns/m, 2000 Ns/m and 2000 Ns/m, respectively. The sub-rail foundation is the long sleeper embedded monolithic track slab. The track superelevation is 90 mm and the curve radius of the line is 350 m. Through the field investigation, it is found that there is side wear on the outer rail of the section, and the corrugation mostly occurs on the inner rail, and the degree of inner rail corrugation is relatively serious. The field picture is shown in Fig. 1.

Rail corrugation is a kind of periodic track irregularity. The existing track irregularity on the actual line is composed of random irregularities with different wavelengths, different phases and different amplitudes, and it is a complex random process related to the line mileage and traffic volume. Therefore, it is limited to use wavelength and wave depth to evaluate corrugation, and it is more appropriate to use statistical parameters in stochastic theory. In this paper, the rail surface roughness level is selected to analyze and evaluate the rail corrugation in the measured section, and the degree of rail corrugation is expressed in the form of one third octave wavelength spectrum. The calculation method of rail surface roughness level Lr is shown in Eq. (1):

$$Lr = 20\lg\left(\frac{r_{\mathrm{rms}}}{r_0}\right), \tag{1}$$

where r_{rms} is the effective value of rail surface corrugation amplitude, μm; r_0 is the reference value of rail surface roughness level, $r_0 = 1$ μm.

The corrugation acquisition instrument CAT (Corrugation Analysis Trolley) is employed to measure the rail surface irregularity, which uses the principle of inertial reference. The data sampling interval is 2 mm, and the measurement speed is 1 m/s. The variation curve of rail surface irregularity

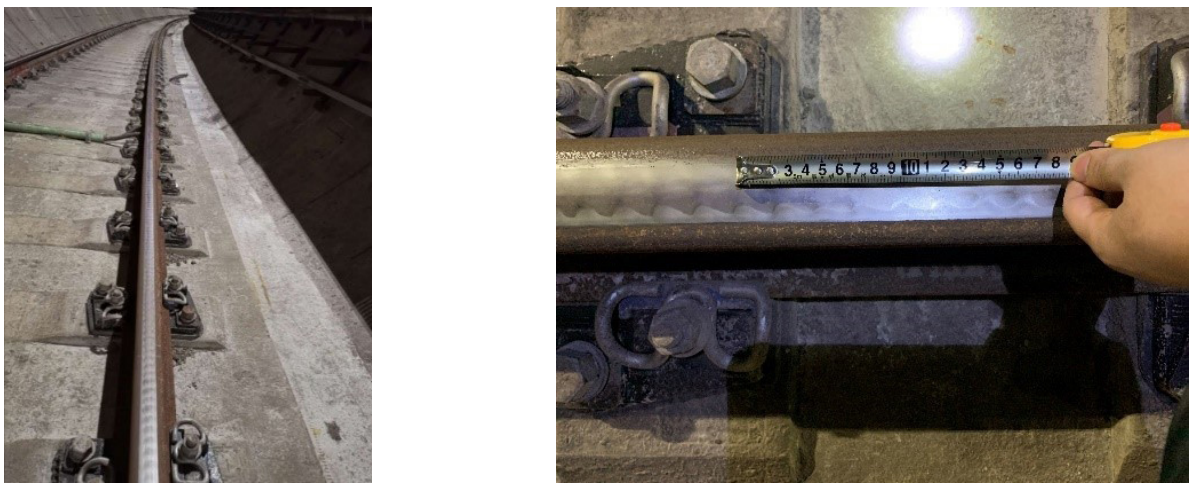

(a) (b)

Fig. 1 Picture of inner rail corrugation: (a) Overall diagram, (b) Detail diagram

in the measured section is shown in Fig. 2, and the corresponding one third octave wavelength spectrum is shown in Fig. 3. As the wavelength of rail corrugation is generally greater than 20 mm (wheel-rail contact patch length), it can be seen from Fig. 3 that the corresponding roughness levels of corrugation wavelengths of inner rail all exceed the rail roughness level limits [20] by more than 3 dB, especially when the wavelength is 63 mm, the corresponding roughness level exceed the limit most, indicating that the characteristic wavelength of inner rail corrugation is 63 mm; the roughness levels corresponding to corrugation wavelengths of outer rail are relatively low, and the roughness levels within the wavelength range of 20~400 mm do not exceed the limits, indicating that the outer rail corrugation is slight or there is no corrugation phenomenon. The above analysis results are consistent with the field investigation. As the running speed of vehicles in the measured section is 55 km/h, the characteristic frequency of inner rail corrugation is 243 Hz according to Eq. (2):

$$f = \frac{1000v}{3.6\lambda}, \tag{2}$$

where f is the corrugation frequency, Hz; v is the vehicle running speed, km/h; λ is the corrugation wavelength, mm.

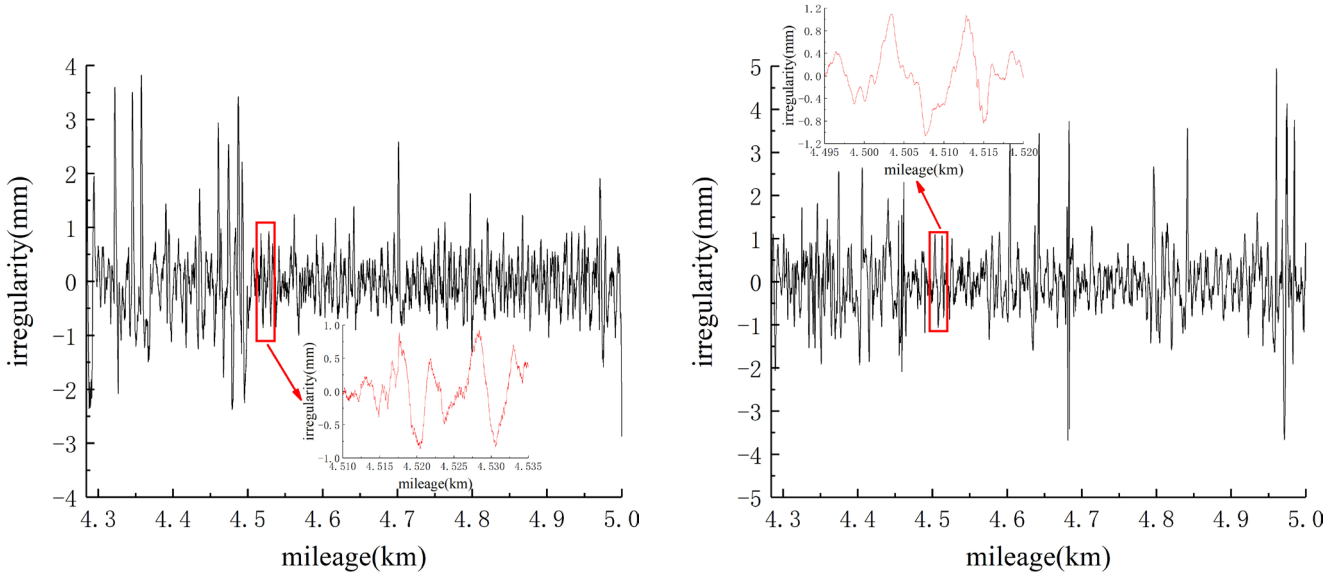

(a) (b)

Fig. 2 Measured rail surface irregularities: (a) Inner rail, (b) Outer rail

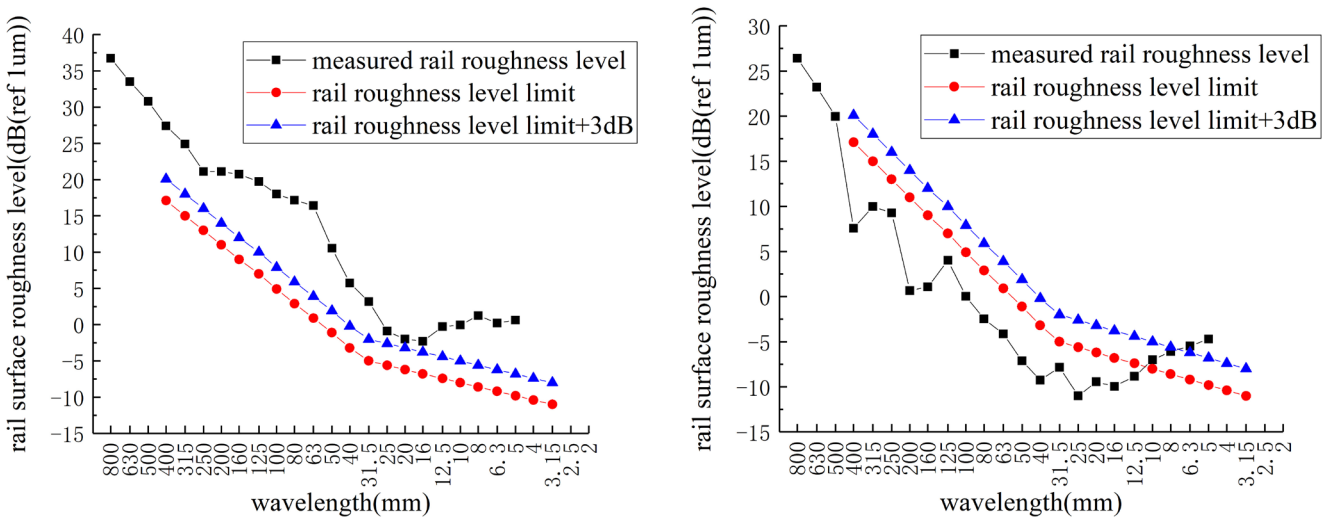

(a) (b)

Fig. 3 Irregularity wavelength spectrums: (a) Inner rail, (b) Outer rail

2.2 Cause theory of rail corrugation

At present, a variety of track vibration-reduction structures are used in metro lines to reduce vibration and noise, but field tests and theoretical analysis show that these structures are more likely to cause abnormal rail corrugation due to their low stiffness characteristics [21]. Rail corrugation is closely related to the fluctuation of wheel-rail normal force. When the vibration frequency of normal force is close to the natural frequency of track structure, the vertical vibration of track structure will be excited, resulting in resonance phenomenon [22].

The above wheel-rail resonance theory is still not enough to explain the cause of rail corrugation. This theory cannot explain why most of the corrugations occur in the curve track, why most of the corrugations occur on the inner rail surface, and why most of the corrugations occur in the curve track with the radius less than 350 m, while when the curve radius is greater than 800 m, rail corrugations rarely occur.

In order to explain the common phenomenon of corrugation occurrence, the generation mechanism of rail corrugation is analyzed in the following. On the curve line, because the inner wheel and the outer wheel are connected through the axle, the radians corresponding to the driving distances of inner wheel and outer wheel are equal during the running of wheelset. When the wheelset passes the circular curve line with a radian α, the distance S_{out} driven by the outer wheel is as follows:

$$S_{out} = \alpha R_{out}, \tag{3}$$

where R_{out} is the curve radius corresponding to the outer rail, m. Similarly, for the inner wheel, the distance S_{inn} is:

$$S_{inn} = \alpha R_{inn}, \tag{4}$$

where R_{inn} is the curve radius corresponding to the inner rail, m. Because of $R_{out} > R_{inn}$ on the curve, there is $S_{out} > S_{inn}$. Set the difference between the driving distances of inner wheel and outer wheel as ΔS, and its expression can be written as

$$\Delta S = S_{out} - S_{inn} = \alpha \left(R_{out} - R_{inn} \right). \tag{5}$$

On the straight line, the driving distances of inner wheel and outer wheel are equal, i.e., $\Delta S = 0$. It can be seen from the above that for the straight track, the driving distances of inner wheel and outer wheel are the same, which are all equal to the rotation arc length of the wheel; for the curved track, the driving distances of inner wheel and outer wheel are no longer equal, the driving distance of outer wheel is equal to the rotating arc length of the wheel, and the driving distance of inner wheel is less than the rotating arc length of the wheel. Therefore, there is a sliding zone with a distance of ΔS for the inner wheel, that is, only when the inner wheel slides on the inner rail surface, can it compensate for the reduced driving distance difference ΔS. However, for the outer wheel, it does not tend to slide, otherwise it will produce a greater distance difference. The above process can be simplified as that the outer wheel passes through the outer rail normally and stably, while the inner wheel needs to slide to keep pace with the outer wheel. Meantime, because the dynamic coefficient of friction is less than the static coefficient of friction [23], once the inner wheel slides, the sliding state will develop further. On the contrary, when the inner wheel slides, the probability of the outer wheel sliding is relatively low. Therefore, due to the frequent sliding action of the inner wheel, the inner rail wear will be more serious.

The above analysis shows that the inner rail tends to be seriously worn. As for why the wear is periodic, that is, how the corrugation is formed, the authors of this paper think that it is mainly related to the unstable vibration of wheelset. The driving distance of outer wheel of the wheelset is longer than that of the inner wheel, which makes the inner wheel tend to slide while the outer wheel still keeps rolling. When the inner wheel slides, the direction of the dynamic friction force exerted by the wheel on the rail is the same as that of the wheel driving, so the direction of the reaction force exerted by the rail on the wheel is opposite to that of the wheel driving, as shown in Fig. 4 (a); since the outer wheel is in the rolling state, the direction of the static friction force exerted by the rail on the wheel is consistent with that of the wheel driving, as shown in Fig. 4 (b). It can be seen from the above that the directions of forces on the contact points between the inner and outer wheels and the rails are opposite, which will lead to torques (the product of the friction force and the rolling circle radius corresponding to the contact point of wheel tread) with opposite directions on the inner and outer wheels. When the torque on the wheel is large enough, the wheel will slide, which will cause the unstable vibration of wheelset. The following will analyze and verify the above cause theory of rail corrugation by dynamics analysis.

3 Calculation and analysis

3.1 Model establishment

The multi-body dynamics software UM (Universal Mechanism) is used to establish the vehicle-track coupling dynamics model. As the running vehicle of the measured line is metro type-A vehicle, the structural parameters of

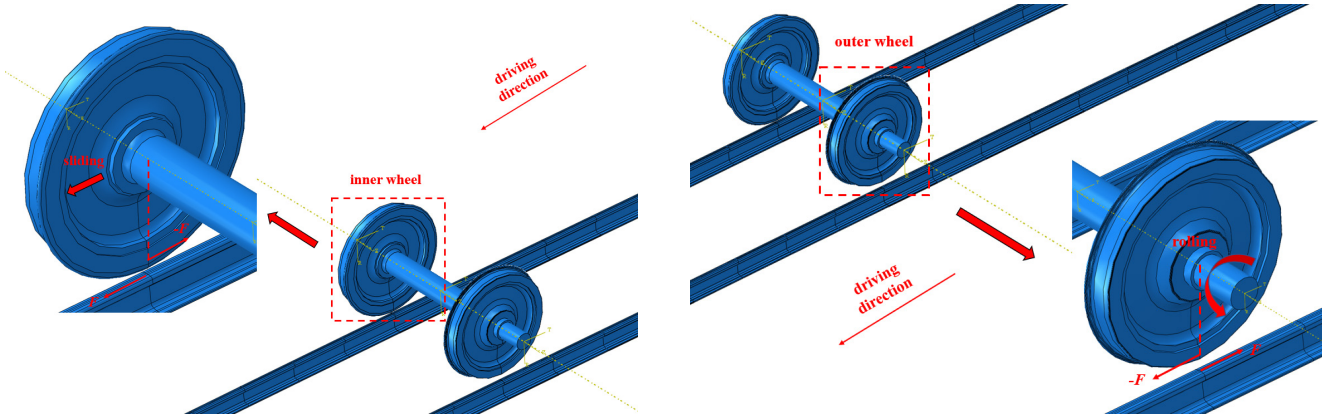

(a) (b)

Fig. 4 Wheel kinematics and force states: (a) Inner wheel, (b) Outer wheel

vehicle model mainly refer to the metro type-A vehicle, as shown in Table 1 [23], and the schematic diagram of vehicle model is shown in Fig. 5. The vehicle model consists of a car body, two bogies and four wheelsets with LM

Table 1 Vehicle structural parameters

parameter	value	unit
bogie mass m_b	4420	kg
body mass m_v	26040	kg
primary suspension vertical stiffness s_{pv}	1.3×10^6	N/m
primary suspension transverse stiffness s_{pt}	5.47×10^5	N/m
primary suspension longitudinal stiffness s_{pl}	5.47×10^5	N/m
primary suspension vertical damping d_{pv}	2400	(N·s)/m
secondary suspension vertical stiffness s_{sv}	2.7×10^5	N/m
secondary suspension transverse stiffness s_{st}	1.15×10^5	N/m
secondary suspension longitudinal stiffness s_{sl}	1.15×10^5	N/m
secondary suspension vertical damping d_{sv}	2.3×10^4	(N·s)/m
moment of inertia of bogie yawing M_{by}	3551	kg·m^2
moment of inertia of bogie rolling M_{br}	1576	kg·m^2
moment of inertia of bogie pitching M_{bp}	4902	kg·m^2
moment of inertia of body yawing M_{vy}	1.1×10^6	kg·m^2
moment of inertia of body rolling M_{vr}	5.88×10^4	kg·m^2
moment of inertia of body pitching M_{vp}	1.1×10^6	kg·m^2
wheel-base bogie d_w	2.5	m
length between bogie pivot centers d_{bc}	15.7	m

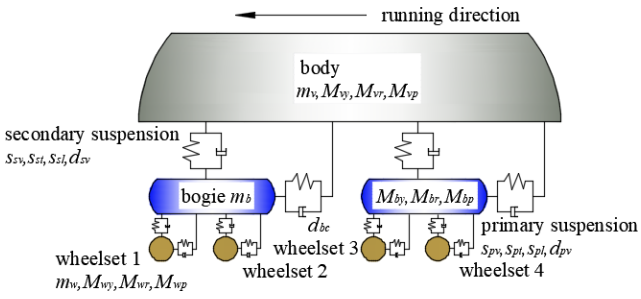

Fig. 5 Schematic diagram of vehicle model

profiles, and their masses and moments of inertia are considered. The secondary suspension between the car body and the bogie and the primary suspension between the bogie and the wheelset are all simulated by spring-damping elements to make the vehicle model closer to the real situation. In the track model, the rail is modeled as the inertial element, the rail type is CHN60 rail, the fastener is modeled as spring-damping elements, and the sub-rail foundation is the concrete sleeper.

The wheel-rail contact adopts the improved algorithm CONTACT. Based on the Duvant-Lions variational principle, the algorithm transforms the friction rolling contact problem into the variational inequality, so as to directly solve the minimum complementary energy in the wheel-rail system [24]. This algorithm divides the contact area into solid elements and boundary elements with the half space assumption to solve the contact problem, and sums the creep force of each element to get the total creep force in the contact area. The static coefficient of friction, i.e., the maximum coefficient of adhesion, is set as 0.3, and the friction/adhesion characteristic complies with the curve of Polach-dry [25]. In addition, it should be noted that the simulation results of the multi-body software can only reflect the friction/adhesion characteristic represented in the wheel-rail-element, which can be used as a reference for practical problems.

According to the above vehicle model, track model and wheel-rail contact model, the vehicle-track coupling model can be established, as shown in Fig. 6.

3.2 Model validation

In this section, the validity of the vehicle-track coupling model is verified by using the field measured rail vertical vibration acceleration. Firstly, the rail surface irregularity is measured by using the CAT. Then, the measured

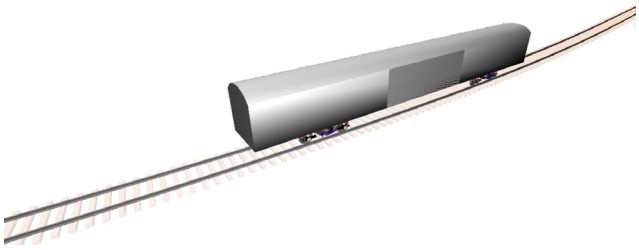

Fig. 6 Vehicle-track coupling model

irregularity is added to the rail model as the initial irregularity. Finally, the simulation and calculation are carried out. The vehicle speed in the model is set as 55 km/h according to the actual situation of the line, and the rail measuring point is located at the top surface of the inner rail bottom (see Fig. 7 for the vibration element). The results of simulation and measurement of rail vertical vibration acceleration at the measuring point are shown in Fig. 7. By calculating the average of the root mean square of the difference between the measured and simulated values at a fixed time, the error between the two is 4.3%. Considering the manual operation in the measurement process and the model simplification in the simulation process, the above error is acceptable and also meets the engineering accuracy requirements, thus verifying the validity of the model.

3.3 Wheel-rail stick-slip characteristics

Based on the vehicle-track coupling model, the line composition is set as (50 m straight line + 50 m transition curve + 200 m circular curve + 50 m transition curve), the radius of circular curve is 350 m, the track superelevation is 90 mm, and the vehicle speed is 55 km/h.

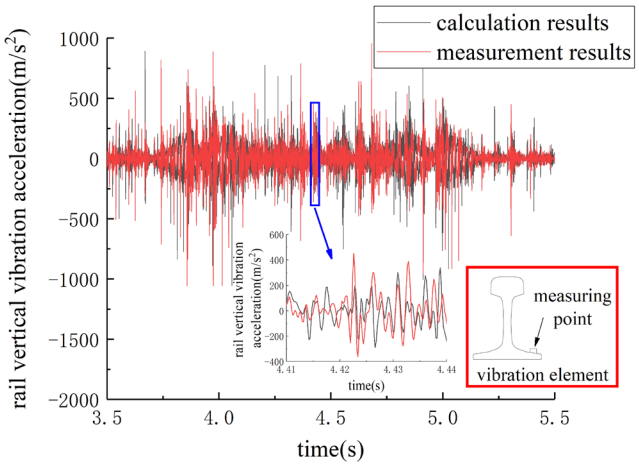

Fig. 7 Comparison of simulation and measurement results

Furthermore, referring to [26], it can be obtained that for curved tracks, when the radius is less than 800 m, the wheel-rail creep force on the outer rail side always reaches saturation, that is, the creep force is equal to the product of wheel-rail coefficient of friction and normal force; when the radius is less than 450 m, the wheel-rail creep force on the inner rail side is always saturated. Therefore, for the circular curve track with a radius of 350 m analyzed in this section, the outputs from the multi-body simulation for the normal force, creep force and creepage are taken as the inputs for the calculation of the corresponding adhesion coefficients. The adhesion coefficients can be obtained by dividing the creep force with the normal force. Combined with the calculation results of wheel-rail creepages, the stick-slip relation curve between adhesion coefficient and creepage can be drawn, as shown in Figs. 8 and 9. The definitions of creepages are expressed in Eq. (6):

$$\xi_x = \frac{(\boldsymbol{v}_w - \boldsymbol{v}_r)\boldsymbol{\tau}_x}{v_0}, \quad \xi_y = \frac{(\boldsymbol{v}_w - \boldsymbol{v}_r)\boldsymbol{\tau}_y}{v_0}, \tag{6}$$

where ξ_x and ξ_y are the longitudinal and transverse creepages; $\boldsymbol{v}_w$ and $\boldsymbol{v}_r$ are the forward velocities of contact points on the wheel and rail; $\boldsymbol{\tau}_x$ and $\boldsymbol{\tau}_y$ are the longitudinal and transverse unit vectors to the contact point; v_0 is the longitudinal velocity of the wheelset.

It can be seen from Fig. 8 that with the increase of transverse creepage, the transverse adhesion coefficient of the inner rail-inner wheel of the leading wheelset gradually decreases, and the wheel-rail stick-slip curve appears a negative slope phenomenon, which indicates that the transverse relative slip of the inner wheel-inner rail occurs. When the inner wheel and inner rail stick, the rail wear is small; when the inner wheel and inner rail slip, the rail wear is large, so with the increase of vehicle running times, the rail corrugation is formed on the inner rail surface. The adhesion coefficients of the other wheel-rail interfaces are positively correlated with the corresponding creepages, and there is no obvious negative slope section, which illustrates that the corresponding wheel-rail interface will not have micro slip, so it is not easy to produce rail corrugation.

According to Fig. 9, it can be obtained that the transverse stick-slip curve of the outer rail-outer wheel of the trailing wheelset has a negative slope phenomenon, while the other wheel-rail stick-slip curves have no obvious negative slope section, indicating that the outer rail-outer wheel of the trailing wheelset will also produce transverse relatively slip, which leads to the formation of outer rail

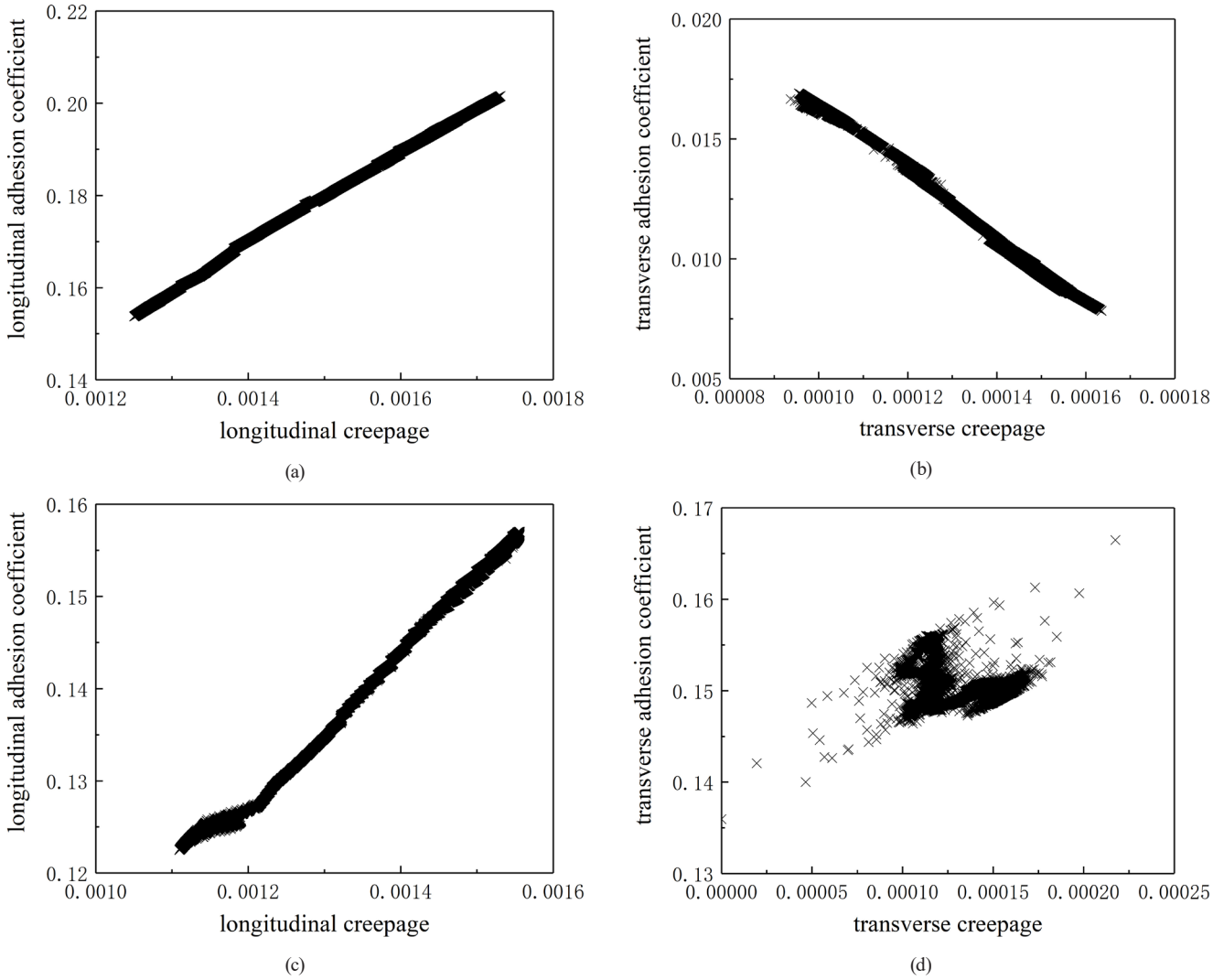

Fig. 8 Wheel-rail stick-slip relation curves of leading wheelset for the curved track with a radius of 350 m: (a) Inner wheel-inner rail longitudinal direction, (b) Inner wheel-inner rail transverse direction, (c) Outer wheel-outer rail longitudinal direction, (d) Outer wheel-outer rail transverse direction

corrugation. However, the adhesion coefficient of 0.070 of the outer rail-outer wheel of the trailing wheelset is greater than that of 0.017 of the inner rail-inner wheel of the leading wheelset. Therefore, the transverse relatively slip of the outer rail-outer wheel of the trailing wheelset is relatively weak and not easy to occur, that is, the outer rail corrugation is relatively slight or not easy to form.

The relationship between wheel-rail stick-slip characteristics and track curve radii will be further discussed in this section, so as to explain the phenomenon that the corrugation mostly occurs on the inner rail of the small radius curve track. The stick-slip curves on the curve track with a radius of 800 m are drawn, as shown in Fig. 10. According to Figs. 8 and 9, it can be seen that the leading wheelset has a greater impact on the formation of rail corrugation, therefore, limited to space, only the wheel-rail stick-slip relation curves of leading wheelset are given below.

It can be seen from Fig. 10 that for the curved track with a radius of 800 m, the variation trends of the stick-slip curves on the inner and outer rail sides are roughly similar, and there is almost no negative slope section in the whole creepage range. The results show that with the increase of curve radius, the wheels on the inner and outer rail sides tend to the complete rolling state, and the sliding wear reduces gradually, thus the occurrence probability of rail corrugation decreases.

The above analysis illustrates that the inner rail wear in the small radius curve is more serious, which is similar to the actual situation of severe inner rail corrugation in the small radius curve, but the corrugation has periodicity. In order to explore the cause of inner rail corrugation, the following will study how the inner rail corrugation has periodic characteristics from the perspective of wheelset-track system modal shapes.

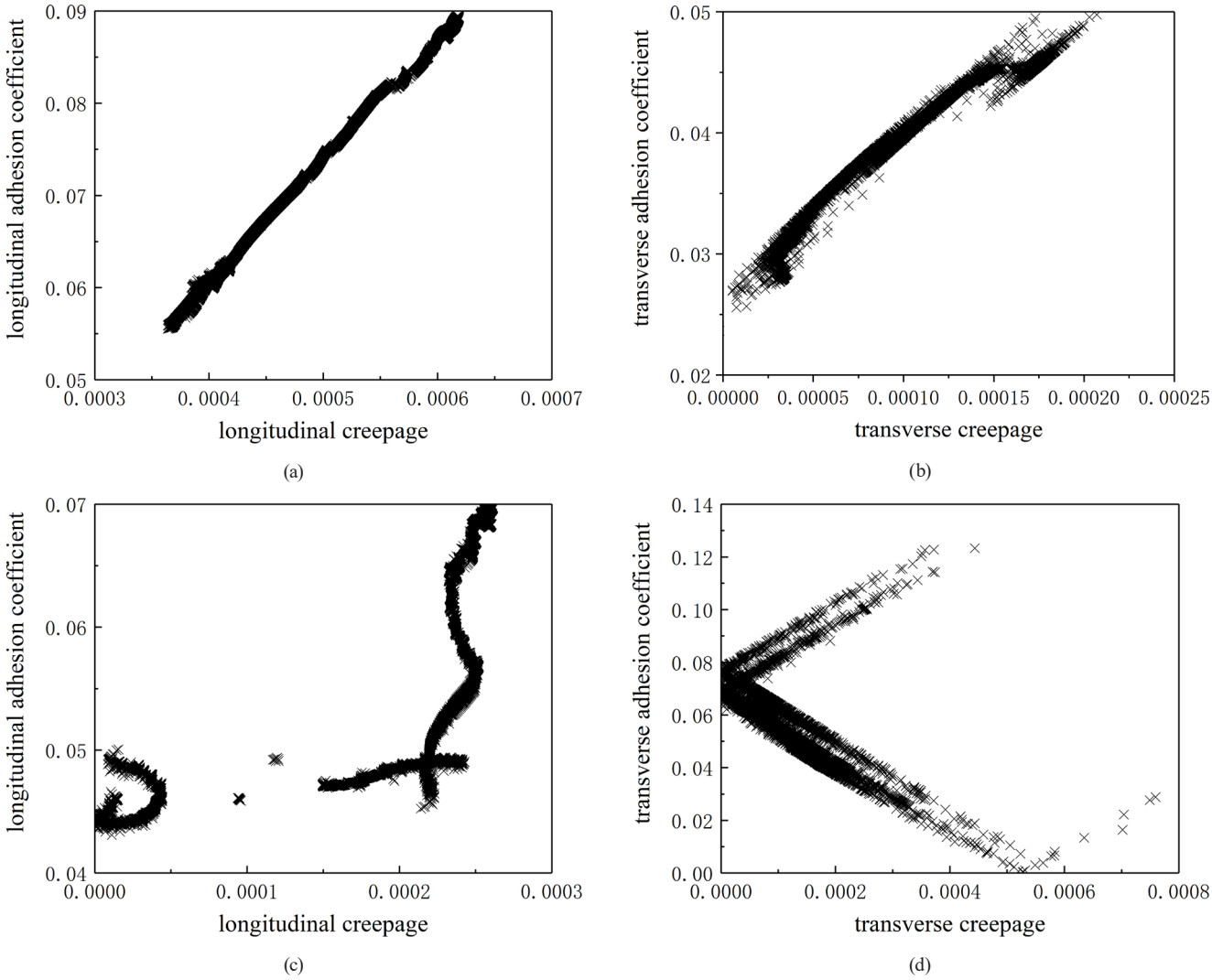

Fig. 9 Wheel-rail stick-slip relation curves of trailing wheelset for the curved track with a radius of 350 m: (a) Inner wheel-inner rail longitudinal direction, (b) Inner wheel-inner rail transverse direction, (c) Outer wheel-outer rail longitudinal direction, (d) Outer wheel-outer rail transverse direction

3.4 Modal characteristics of wheelset-track system

By using the finite element software ABAQUS, the three-dimensional solid model of wheelset-track system is established, which mainly includes a wheelset and two rails. Both ends of the rail are fixed constraints, and the rail is connected to the sub-rail foundation through fasteners (spring-damping elements), as shown in Fig. 11. In the model, the nominal rolling circle radius of the wheel is 420 mm, the tread type of the wheel is LM wear type, and the rail adopts CHN60 rail. The wheel and rail are connected by the friction coupling, and the wheel-rail coefficient of friction is set as 0.3. The track gauge is 1435 mm, the length of the track center line is 36 m, and the corresponding curve radius is 350 m. The structural parameters of wheelset-track system refer to [26].

According to [27], it can be seen that when the negative slope characteristic of stick-slip curve appears in the wheel-rail system, the wheelset will produce unstable self-excited vibration. In view of this, the modal analysis of the above three-dimensional wheelset-track system model is carried out in this section to study the natural vibration characteristics of wheelset-track system. On the basis of Section 2.1, the characteristic frequency of inner rail corrugation is 243 Hz, the frequency close to that in modal analysis results is 251 Hz, and the corresponding vibration mode is shown in Fig. 12. It can be seen from Fig. 12 that the inner rail has obvious bending-torsional vibration, while the outer rail has no remarkable vibration. Furthermore, the vibration mode of the wheelset at this frequency is extracted, as shown in Fig. 13, and it is easy to see that the bending vibration of wheel discs on the inner and outer rail sides occurs. By analyzing Figs. 12 and 13, it can be concluded that the coupling vibration of inner wheel-inner rail is significantly greater than that of outer wheel-outer rail, indicating that the inner wheel-inner rail is more prone to unstable vibration. Combined

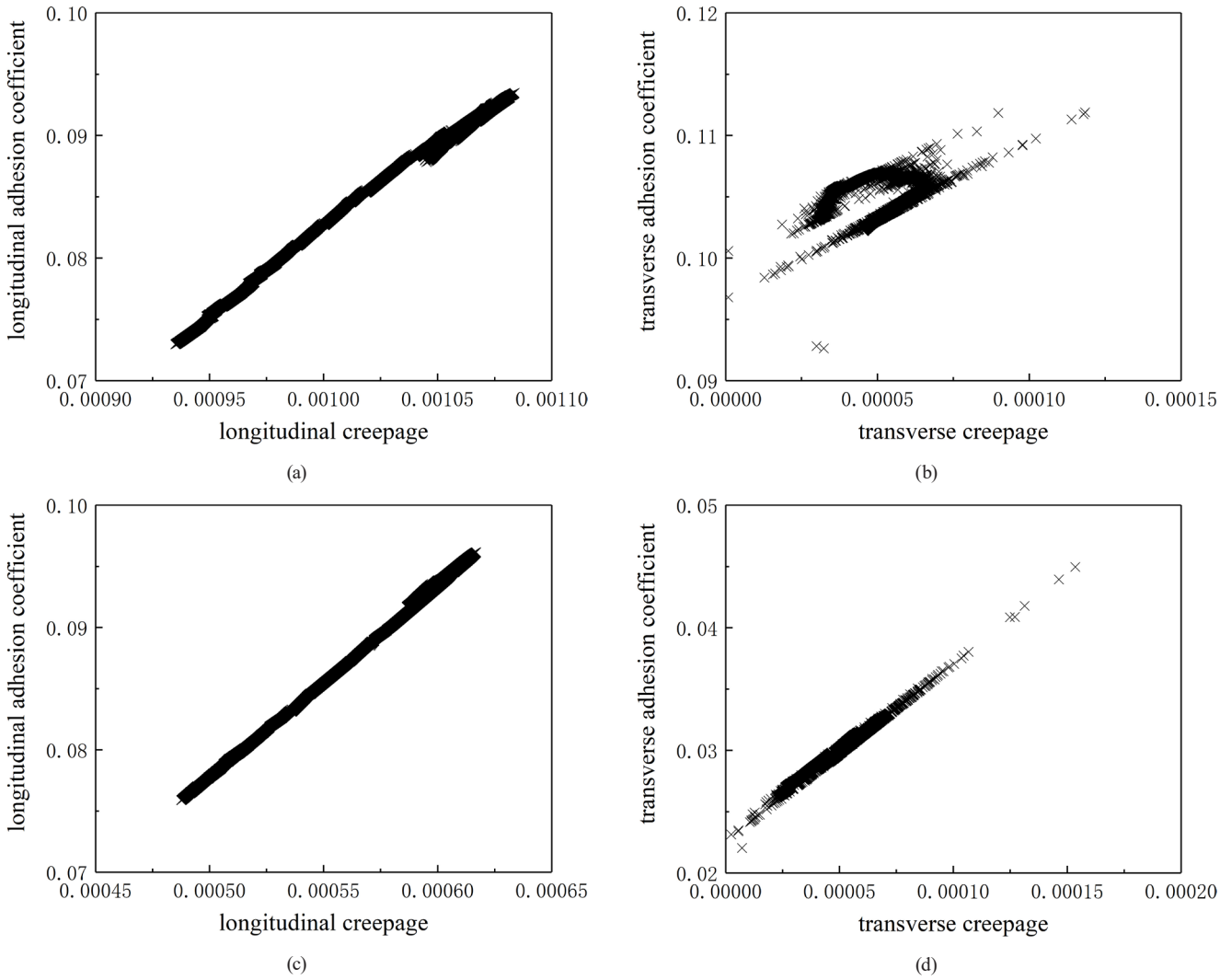

Fig. 10 Wheel-rail stick-slip relation curves of leading wheelset for the curved track with a radius of 800 m: (a) Inner wheel-inner rail longitudinal direction, (b) Inner wheel-inner rail transverse direction, (c) Outer wheel-outer rail longitudinal direction, (d) Outer wheel-outer rail transverse direction

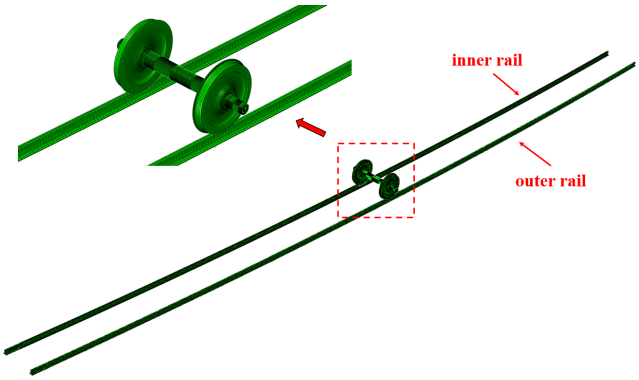

Fig. 11 Wheelset-track finite element model

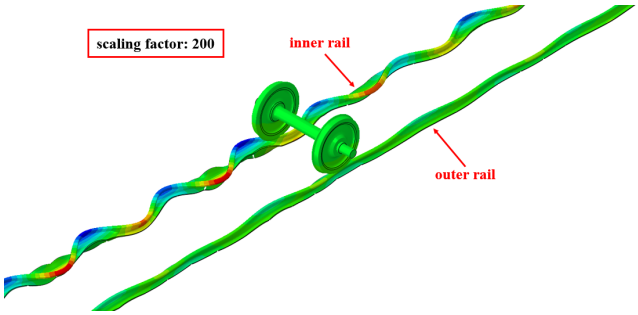

Fig. 12 Vibration mode of wheelset-track system corresponding to the frequency of 251 Hz

with the analysis results of wheel-rail stick-slip characteristics, it can be obtained that the inner rail is more prone to rail corrugation, which is consistent with the actual situation of rail corrugation on metro lines. Meanwhile, it also verifies the cause theory of rail corrugation described in Section 2.2. Therefore, the main cause of rail corrugation is the coupling effect of wheel discs bending vibration and inner rail bending-torsional vibration under the condition of wheel-rail system with stick-slip negative slope. There are some related researches in [28–30], such as the self-excited vibration of wheel-rail system and the

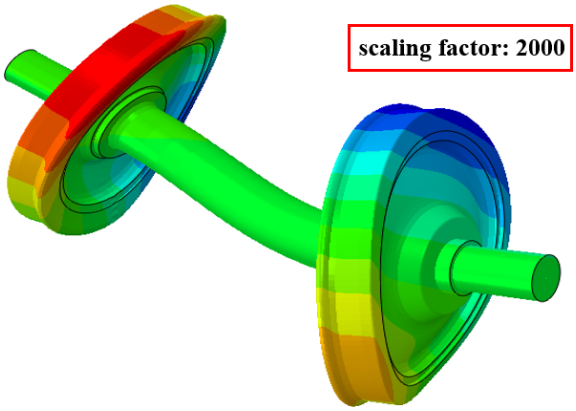

Fig. 13 Vibration mode of wheelset corresponding to the frequency of 251 Hz

corresponding bending and torsional vibration modes, however, compared with those, this paper further analyzes the contact creep characteristics of inside and outside wheel-rail systems of leading and trailing wheelsets in detail. Meanwhile, combined with the modal analysis, the formation mechanism of rail corrugation is comprehensively explained in the presented paper.

4 Conclusions

Based on the measured corrugation on the actual line, this paper first analyzes the cause of rail corrugation theoretically. Then, the vehicle-track coupling model is used to study the stick-slip characteristics of wheel-rail system. Finally, through the modal analysis of wheelset-track system, combined with the wheel-rail stick-slip relation, the cause of rail corrugation is explained. The following conclusions can be drawn:

1. The analysis of measured data shows that the inner rail corrugation is serious, and its characteristic wavelength is 63 mm; the outer rail corrugation is slight or there is no corrugation.
2. When the vehicle runs in the curve section with a radius of 350 m, the transverse stick-slip curve on the inner rail-inner wheel of the leading wheelset has obvious negative slope characteristics, which makes the inner wheel easy to slide on the inner rail surface and aggravates the inner rail wear; there are also negative slope sections of the stick-slip curve on the outer rail-outer wheel of the trailing wheelset, but the adhesion coefficient is relatively large, indicating that the outer wheel does not slide significantly and the wear is relatively small.
3. With the increase of the line curve radius, the negative slope phenomenon of stick-slip curves on the inner and outer rail sides shows a decreasing trend, which indicates that the sliding wear of the wheel gradually reduces, and thus the occurrence probability of rail corrugation decreases.
4. Combining wheel-rail stick-slip characteristics and modal analysis, it can be seen that the coupling effect of wheel discs bending vibration and inner rail bending-torsional vibration is the main cause of rail corrugation under the condition of wheel-rail system with stick-slip negative slope.

References

[1] Grassie, S. L. "Rail corrugation: characteristics, causes, and treatments", Proceedings of the Institution of Mechanical Engineers, Part F: Journal of Rail and Rapid Transit, 223(6), pp. 581–596, 2009. https://doi.org/10.1243/09544097JRRT264

[2] Feller, H. G., Walf, K. "Surface analysis of corrugated rail treads", Wear, 144(1–2), pp. 153–161, 1991. https://doi.org/10.1016/0043-1648(91)90012-J

[3] Liu, Q. Y., Wang, X. Q., Zhou, Z. R. "钢轨表面波浪形磨损研究" (An investigation of rail corrugation), Tribology, 18(4), pp. 50–53, 1998. (in Chinese)

[4] Li, X., Li, W., Wen, Z. F., Jin, X. S., Wang, H. Y., Wu, L. "普通短轨枕轨道结构钢轨波磨初步研究" (Preliminary study on the rail corrugation of the fixed-dual short sleepers track), Journal of Mechanical Engineering, 49(2), pp. 109–115, 2013. (in Chinese) https://doi.org/10.3901/JME.2013.02.109

[5] Xiao, X. B., Wen, Z. F., Jin, X. S., Sheng, X. Z. "Effects of track support failures on dynamic response of high speed tracks", International Journal of Nonlinear Sciences and Numerical Simulation, 8(4), pp. 615–630, 2007. https://doi.org/10.1515/IJNSNS.2007.8.4.615

[6] Liu, W. F., Liu, W. N., Wu, Z. Z., Zhang, H. G. "北京地铁剪切型减振器扣件钢轨波磨治理的试验研究" (Test study on treating rail corrugation for egg fastener in Beijing metro), Journal of Mechanical Engineering, 51(21), pp. 73–79, 2015. (in Chinese) https://doi.org/10.3901/JME.2015.21.073

[7] Li, X., Li, W., Shen, Y. Y., Wen, Z. F., Jin, X. S. "基于轨道振动理论的梯形轨枕轨道钢轨波磨研究" (Study on the rail corrugation of the ladder-type sleepers track based on the track vibration theory), Journal of Mechanical Engineering, 52(22), pp. 121–128, 2016. (in Chinese) https://doi.org/10.3901/JME.2016.22.121

[8] Li, X., Ren, Z. S., Xu, N. "地铁小半径曲线段钢弹簧浮置板轨道的钢轨波磨研究" (Study on rail corrugation of steel spring floating slab track on subway with small radius curve track), Journal of the China Railway Society, 39(8), pp. 70–76, 2017. (in Chinese) https://doi.org/10.3969/j.issn.1001-8360.2017.08.010

[9] Li, W., Wen, Z. F., Wang, H. Y., Zhao, X., Wang, P. "地铁钢轨波磨演化过程中的特性分析" (Analysis on the evolution characteristics of rail corrugation on a metro), Journal of Mechanical Engineering, 54(4), pp. 70–78, 2018. (in Chinese) https://doi.org/10.3901/JME.2018.04.070

[10] Shen, G., Zhang, X. H., Guo, M. H. "地铁曲线波浪型磨耗的机理分析" (Theoretical study on rail corrugation on curved track of metro systems), Journal of Tongji University (Natural Science), 39(3), pp. 381–384, 2011. (in Chinese)
https://doi.org/10.3969/j.issn.0253-374x.2011.03.013

[11] Yao, H. M., Shen, G., Gao, L. J. "基于试验验证的磨耗型钢轨波磨形成机理" (Formation mechanism of worn profile rail corrugation based on experimental verification), Journal of Tongji University (Natural Science), 46(10), pp. 1427–1432, 2018. (in Chinese)
https://doi.org/10.11908/j.issn.0253-374x.2018.10.015

[12] Suda, Y. "Effects of vibration system and rolling conditions on the development of corrugations", Wear, 144(1–2), pp. 227–242, 1991.
https://doi.org/10.1016/0043-1648(91)90017-O

[13] Ahlbeck, D. R., Daniels, L. E. "Investigation of rail corrugations on the Baltimore metro", Wear, 144(1–2), pp. 197–210, 1991.
https://doi.org/10.1016/0043-1648(91)90015-M

[14] Bellette, P. A., Meehan, P. A., Daniel, W. J. T. "Validation of a tangent track corrugation model with a two disk test rig", Wear, 271(1–2), pp. 268–277, 2011.
https://doi.org/10.1016/j.wear.2010.10.020

[15] Eadie, D. T., Santoro, M., Oldknow, K., Oka Y. "Field studies of the effect of friction modifiers on short pitch corrugation generation in curves", Wear, 265(9), pp. 1212–1221, 2008.
https://doi.org/10.1016/j.wear.2008.02.028

[16] Meehan, P. A., Batten, R. D., Bellette, P. A. "The effect of non-uniform train speed distribution on rail corrugation growth in curves/corners", Wear, 366–367, pp. 27–37, 2016.
https://doi.org/10.1016/j.wear.2016.05.009

[17] Qian, W. J., Huang, Z. Q. "蠕滑力饱和条件下钢轨吸振器抑制短波波磨的理论研究" (Theoretical study on the suppression of short pitch rail corrugation induced vibration by rail vibration absorbers under saturated creep forces condition), Journal of Vibration and Shock, 38(14), pp. 68–73+111, 2019. (in Chinese)
https://doi.org/10.13465/j.cnki.jvs.2019.14.010

[18] Hu, W. P., Wang, P., Chen, G. X., Hu, Y., Cui, X. L., Peng, J. F., Zhu, M. H. "Experimental study on corrugation of a sliding surface caused by frictional self-excited vibration", Tribology Transactions, 59(1), pp. 8–16, 2016.
https://doi.org/10.1080/10402004.2015.1041628

[19] Jin, X. S., Li, X., Li, W., Wen, Z. F. "铁路钢轨波浪形磨损研究进展" (Review of rail corrugation progress), Journal of Southwest Jiaotong University, 51(2), pp. 264–273, 2016. (in Chinese)
https://doi.org/10.3969/j.issn.0258-2724.2016.02.006

[20] European Committee for Standardization "BS EN ISO 3095:2013 Acoustics - Railway applications - Measurement of noise emitted by railbound vehicles", British Standards Institution, London, UK, 2013.

[21] Lu, Y. "地铁小半径曲线钢轨磨耗的防治措施" (Measures against rail wear on subway small radius curve section), Urban Mass Transit, 21(1), pp. 68–71, 2018. (in Chienese)
https://doi.org/10.16037/j.1007-869x.2018.01.016

[22] Liu, X., Wang, P. "Investigation of the generation mechanism of rail corrugation based on friction induced torsional vibration", Wear, 468–469, 203593, 2021.
https://doi.org/10.1016/j.wear.2020.203593

[23] Lei, Z. Y., Wang, Z. Q., Li, L., Geng, C. Z. "地铁普通扣件钢轨波磨特性" (Rail corrugation characteristics of the common fastener track in metro), Journal of Tongji University (Natural Science), 47(9), pp. 1334–1340, 2019. (in Chinese)
https://doi.org/10.11908/j.issn.0253-374x.2019.09.014

[24] Jin, X. S., Xue, B. Y. "三维非赫兹滚动接触理论在轮轨滚动接触中的应用——TPLR 的编制及应用" (Application of three-dimensional non-Hertzian rolling contact theory to wheel/rail rolling contact-compilation and application of TPLR), Journal of Southwest Jiaotong University, 32(4), pp. 407–412, 1997. (in Chinese)

[25] Polach, O. "Creep forces in simulations of traction vehicles running on adhesion limit", Wear, 258(7–8), pp. 992–1000, 2005.
https://doi.org/10.1016/j.wear.2004.03.046

[26] Wang, Z., Lei, Z., Zhao, Y., Xu, Y. "Rail corrugation characteristics of Cologne Egg fastener section in small radius curve", Shock and Vibration, 2020, 1827053, 2020.
https://doi.org/10.1155/2020/1827053

[27] Sun, L. X., Yao, J. W., Hou, F. G. "轮轨干摩擦下的轮对横向自激振动机理" (Lateral self-excited vibration mechanism of wheelset subjected to wheel/rail dry friction contact system), China Railway Science, 33(5), pp. 60–67, 2012. (in Chinese)
https://doi.org/10.3969/j.issn.1001-4632.2012.05.10

[28] Bogacz, R., Frischmuth, K. "On some new aspects of contact dynamics with application in railway engineering", Journal of Theoretical and Applied Mechanics, 50(1), pp. 119–129, 2012.

[29] Noga, S., Bogacz, R., Markowski, T. "Vibration analysis of a wheel composed of a ring and a wheel-plate modelled as a three-parameter elastic foundation", Journal of Sound and Vibration, 333(24), pp. 6706–6722, 2014.
https://doi.org/10.1016/j.jsv.2014.07.019

[30] Bogacz, R., Kurnik, W. "On kinematic and self-excited rail vehicle-track interaction", Archive of Applied Mechanics, 88(1–2), pp. 193–201, 2018.
https://doi.org/10.1007/s00419-017-1298-x